

On the Orbits of Similarity Classes of Tetrahedra Generated by the Longest-Edge Bisection Algorithm

Jérôme Michaud and Sergey Korotov

December 9, 2025

Division of Mathematics and Physics, UKK, Mälardalen University, Västerås, Sweden
 emails: jerome.michaud@mdu.se, sergey.korotov@mdu.se

Abstract

In this work, we study the dynamics of similarity classes of tetrahedra generated by the longest-edge bisection (LEB) algorithm. Building on the normalization strategy introduced by Perdomo and Plaza for triangles in [1, 2], we construct a canonical representation of tetrahedra in a normalized space embedded in the product of the hyperbolic half-plane and the hyperbolic half-space model. This representation allows us to define the left and right refinement maps, Φ_L and Φ_R , acting on the space of normalized tetrahedral shapes, and to study their iterative orbits as discrete dynamical systems. Using these maps, we show that the orbit of the space-filling Sommerville tetrahedron contains only 4 similarity classes, 3 of which form an attractive cycle corresponding to the orbit of the path tetrahedron. We also show that small perturbations of elements in those orbits still lead to finite orbits. In addition, we study small perturbations of the regular tetrahedron and show that their orbits are also finite. Extensive numerical exploration of orbits for the other types of tetrahedra suggests that the LEB algorithm does not produce degenerating tetrahedra. Our framework provides a geometric and dynamical foundation for analyzing the shape evolution of tetrahedral meshes and offers a possible route toward an analytic proof of the non-degeneracy property for the tetrahedral partitions generated by the LEB refinements. This property is highly desired in e.g. the finite element methods (FEMs).

Keywords: bisection algorithm, finite element method, tetrahedral partition, mesh regularity, dynamical system, hyperbolic geometry

AMS Classification: 65M50, 65N50, 65N30

1 Introduction

When solving boundary value problems using the finite element method (FEM), the computational domain is usually divided into small, non-overlapping, and often simplex-shaped, elements (whose total set is commonly called mesh). Ideally, we should also have a suitable refinement technique which produce smaller and smaller elements (i.e. finer meshes). In three dimensions, this means partitions of the domain of interest into tetrahedra whose shape and quality play a crucial role in the accuracy and stability of the numerical approximation [3]. In particular, to guarantee the optimal convergence rates and bounded interpolation constants, it is necessary that the generated families of tetrahedral partitions remain *regular* or *strongly regular* in the sense of Zlámal, see [4–6].

Among the various refinement techniques developed for generating adaptive and hierarchical FEM meshes, the *longest-edge bisection* (LEB) algorithm has emerged as one of the most widely used and conceptually simplest strategies. Originally introduced in the context of solving nonlinear systems of equations by Stynes [7] and later adopted for mesh generation/refinements in various works by Rivara, see e.g. [8, 9], the method recursively bisects each simplex by a plane passing through the midpoint of its longest edge and the remaining vertices. In two dimensions, the algorithm has been shown to produce a finite number of similarity classes of triangles and thus to preserve the non-degeneracy of the meshes [10, 11]. However, in three dimensions,

the situation is considerably more complicated. While the method idea can be straightforwardly extended to tetrahedral meshes, a general proof of regularity remains elusive for several decades [12, 13].

Recent studies on the topic have therefore concentrated on the classification of tetrahedral elements generated by repeated application of the LEB algorithm according to their *similarity classes*. Each refinement step produces new tetrahedra whose shape can be characterized up to translation, rotation, reflection, and scaling. If the number of distinct similarity classes produced during refinement is finite, then regularity follows immediately. This approach has led to a number of algorithmic and computational investigations. In particular, Suárez, Trujillo-Pino, and Moreno [14] developed an integer-arithmetic algorithm that normalizes tetrahedra by their ordered sextuple of squared edge lengths, allowing an exact comparison of similarity classes as long as squared edge lengths are integers. In general this normalization procedure is not exact, but numerically precise enough to identify similarity classes. They call their algorithm the *Similarity classes longest-edge bisection* (SCLEB) algorithm. Trujillo-Pino *et al.* [15] refined this analysis and proved that nearly equilateral tetrahedra generate at most thirty-seven distinct similarity classes under successive bisections. Other related works have examined special cases, such as the regular or trirectangular tetrahedra, within the framework of the eight-tetrahedron partition [16]. These approaches have significantly advanced the enumeration of similarity classes but remain largely combinatorial in nature. They rely on edge-length representations and discrete comparison criteria, which do not easily lend themselves to analytical study of the underlying geometric transformations induced by the LEB process.

In contrast, the situation in two dimensions has benefited from a *geometric normalization* of triangular elements. Perdomo and Plaza [1, 2] introduced a space of normalized triangles endowed with a hyperbolic metric in the Poincaré half-plane. In this framework, each triangle corresponds to a point in a canonical region of the hyperbolic plane, and the refinement operation acts as an isometry of that space. This geometric viewpoint allows for both a continuous description of the discrete refinement process and an analytic proof of non-degeneracy for the resulting families of triangulations.

The aim of the present work is to extend this geometric perspective to the three-dimensional setting. We introduce a normalization procedure that maps each tetrahedral element to a canonical representative in a space of *normalized tetrahedra* obtained by selecting a base face to be mapped onto Perdomo and Plaza's space of triangle [1, 2] and the fourth vertex to the upper half-space using shape preserving transformations. The resulting representation of a tetrahedron can be seen as a point in the product space of the Poincaré half-plane \mathbb{H}^2 and the Poincaré half-space \mathbb{H}^3 models. Using the induced product metric, we obtain a canonical metric space of tetrahedra. Within this space, the LEB refinement step is represented by two maps, Φ_L and Φ_R , corresponding to the left and right sub-tetrahedra generated by bisecting the longest edge. The iterative behavior of these maps defines orbits of normalized tetrahedra whose closure characterizes the long-term dynamics of the refinement process. By studying these orbits, we seek to identify closed families of tetrahedra, describe their orbits, and provide numerical evidence of boundedness and non-degeneracy of the resulting partitions.

This normalization framework thus connects the algorithmic classification of similarity classes of Suárez, Trujillo-Pino, and Moreno [14] with a geometric and dynamical-systems interpretation of the refinement process. It offers a unified setting in which both analytical and numerical investigations of tetrahedral regularity can be pursued.

2 Normalizing and visualizing the similarity classes of tetrahedra

In this section, we introduce a normalization procedure inspired by the work of Perdomo and Plaza [1, 2] for triangles. The idea is to select one of six faces of the tetrahedron as its canonical base and send that face to the canonical space of triangles by translation, rotations, and scaling operations, hence preserving the shape of the tetrahedron. When doing such a transformation, the fourth vertex can have either a positive or negative third component. Therefore, similarly to [1, 2], we also use a reflection (if needed) to ensure that the fourth vertex is finally mapped to the upper half-space. Using such a normalization procedure, we can study the longest-edge bisection (LEB) refinement process both analytically and numerically as a discrete dynamical system. Furthermore, such type of normalization provides a natural way to visualize the orbit of a given tetrahedron under the LEB refinement process. Compared to other normalization approaches, such as that of [14, 15] based on the square length of edges, our normalization procedure uniquely maps similarity classes

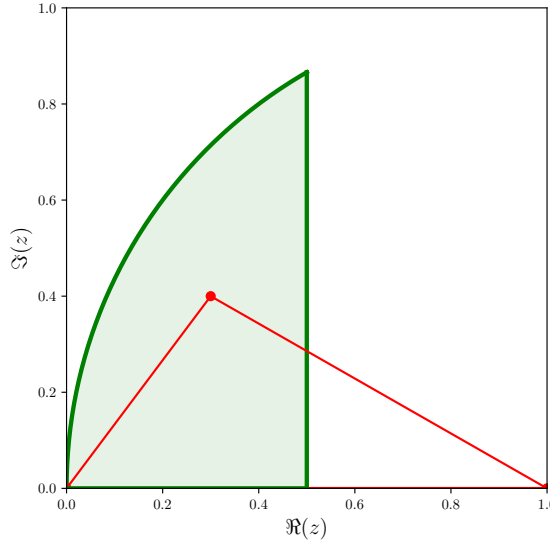


Figure 1: An illustration for the canonical space of triangles. The set \mathcal{B} , of admissible positions for the third vertex, is colored in green.

to a compact metric space and provides a natural and intuitive visualization of the underlying dynamics.

2.1 The canonical space of tetrahedra

Definition 2.1. Let \mathcal{S} be the space of all non-degenerate tetrahedra. Two tetrahedra $T_1 \in \mathcal{S}$ and $T_2 \in \mathcal{S}$ are called shape similar if and only if there exists an isometry $R \in O(3)$, a translation vector b , and a positive scalar $\lambda > 0$, such that $T_2 = b + \lambda R T_1$, and we write $T_1 \sim T_2$. The space of similarity classes is then defined as \mathcal{S}/\sim .

The normalization procedure is, in general, about selecting a suitable (canonical) representative of each class in \mathcal{S}/\sim . In order to describe that in detail, we need to introduce some extra definitions and denotation.

First, we recall the concept of the so-called canonical space of triangles, see [1].

Definition 2.2. The canonical space of triangles consists of triangles having $(0, 0)$ and $(0, 1)$ as two (fixed) vertices in the complex plane, and for which the third vertex lies in the set

$$\mathcal{B} := \{z \in \mathbb{C} \mid \Im(z) > 0, 0 < \Re(z) \leq \frac{1}{2}, |z - 1| \leq 1\},$$

where $\Im(z)$ is the imaginary part of z and $\Re(z)$ is the real part of z .

Remark 2.1. From the above definition, it follows that the edge connecting 0 and 1 (of the length 1) is the longest (or one of the longest ones), and the edge connecting 0 and z , of the length $|z|$, is the shortest (or one of the shortest ones) for all triangles from the canonical space of triangles, see Figure 1.

Now, each canonical tetrahedron will be defined as that having one of its faces in the canonical space of triangles, which means that three of its vertices are the points 0 , 1 , and z . The set of possible positions for the fourth vertex $\mathcal{V}(z)$, provided z is fixed, is described in the next definition.

Definition 2.3. The set of possible positions of the fourth-vertex $\mathcal{V}(z)$ is defined as

$$\mathcal{V}(z) := \{(w, t) \in \mathbb{C} \times \mathbb{R}_+ \mid |z|^2 \leq |w|^2 + t^2 \leq 1, |z|^2 \leq |w - 1|^2 + t^2 \leq 1, |w - z|^2 + t^2 \leq 1\}.$$

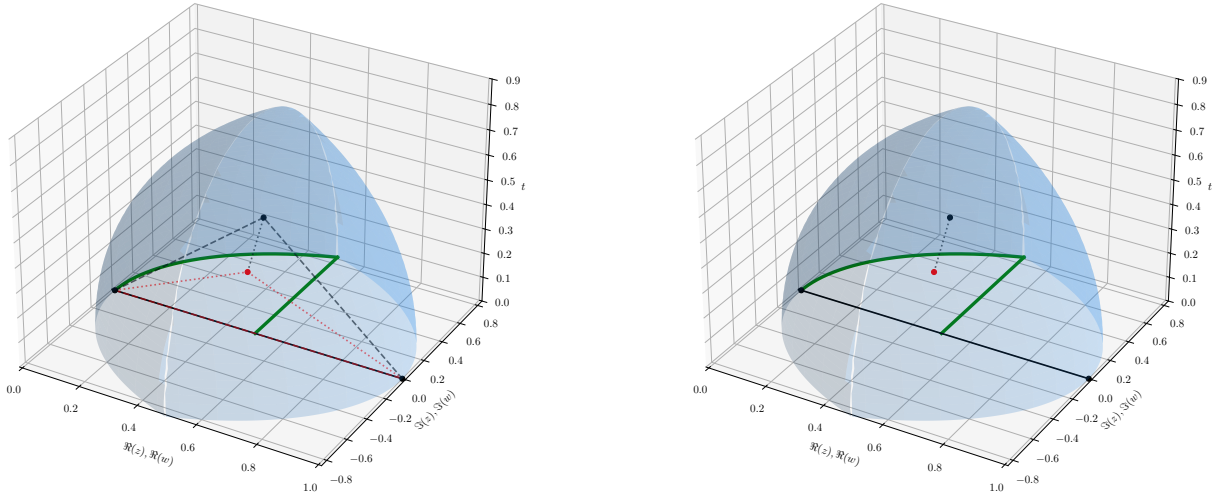


Figure 2: Left: an example of a canonical tetrahedron. The red point is the normalized representation of the canonical base and the black point is the remaining vertex. All the edges of the tetrahedron are also displayed. Right: same figure, but only the edge carrying information is presented.

If $z = z_1 + z_2 i$ and $w = w_1 + w_2 i$, then each canonical tetrahedron is uniquely associated with a tetrahedron with vertices $(0, 0, 0)$, $(1, 0, 0)$, $(z_1, z_2, 0)$, and (w_1, w_2, t) .

Definition 2.4. *The canonical space of tetrahedra \mathcal{T} is defined as*

$$\mathcal{T} := \{(z, (w, t)) \in \mathcal{B} \times \mathcal{V}(z)\}.$$

Elements of \mathcal{T} are denoted by τ , possibly with indices.

An example of visualization for canonical tetrahedra generalizing the case of canonical triangles from [1] is illustrated in Figure 2. In addition to the space of triangles marked by the green color, we added the intersection of two spheres of radius 1 centered at $(0, 0, 0)$ and at $(1, 0, 0)$ in the upper half-space. Such a visual representation of all tetrahedra generated by LEB will be used in the rest of this paper.

In the spirit of [1, 2], we can endow \mathcal{T} with a metric by using the fact that $\mathcal{T} \subset \mathbb{H}^2 \times \mathbb{H}^3$ and defining the product metric.

Definition 2.5. *Let $\mathcal{T} \subset \mathbb{H}^2 \times \mathbb{H}^3$, with points $(z, (w, t))$, $z \in \mathcal{B} \subset \mathbb{H}^2$, $(w, t) \in \mathcal{V}(z) \subset \mathbb{H}^3$. The product metric is:*

$$ds^2 = \frac{|dz|^2}{(\Im(z))^2} + \frac{|dw|^2 + dt^2}{t^2}.$$

Definition 2.6. *The distance between two points $\tau_1 = (z_1, (w_1, t_1)), \tau_2 = (z_2, (w_2, t_2)) \in \mathcal{T}$ is given by*

$$d_{\mathcal{T}}(\tau_1, \tau_2) = \sqrt{d_{\mathbb{H}^2}(z_1, z_2)^2 + d_{\mathbb{H}^3}((w_1, t_1), (w_2, t_2))^2}.$$

Here the hyperbolic distances are:

$$\cosh d_{\mathbb{H}^2}(z_1, z_2) = 1 + \frac{|z_1 - z_2|^2}{2 \Im(z_1) \Im(z_2)},$$

$$\cosh d_{\mathbb{H}^3}((w_1, t_1), (w_2, t_2)) = \frac{|w_1 - w_2|^2 + t_1^2 + t_2^2}{2 t_1 t_2}.$$

2.2 Normalization procedure

Let $T \in \mathcal{S}$ be a non-degenerate tetrahedron. Our normalization procedure maps a well-chosen face with vertices denoted by A, B, C to \mathcal{B} and the vertex D to $\mathcal{V}(z)$, hence, mapping T to an element τ of \mathcal{T} .

Definition 2.7. *The normalization procedure consists of the following steps:*

1. **Selection of the base face and labeling of vertices.** Let us assume that the edge AB is the longest edge of T , and let AC be the shortest among four edges adjacent to AB . If the ambiguity is still not resolved, the face with the smallest angle $\angle BAC$ is chosen. If the ambiguity is still not resolved, the choice is arbitrary and will lead to the same normalization. The face ABC is then selected as the base.
2. **Rigid motion and scaling.** Apply a translation, rotation and scaling so that A is mapped to $(0, 0, 0)$ and B to $(1, 0, 0)$, and the base face ABC lies in the plane $\{x_3 = 0\}$ with C in the upper half-plane ($x_2 > 0$). In practice, let us define $\mathbf{a}, \mathbf{b}, \mathbf{c}$, and \mathbf{d} the vectors corresponding to the vertices A, B, C and D .
 - (a) Translate A to the origin. The coordinates of the other vertices are then defined by $\mathbf{b}' = \mathbf{b} - \mathbf{a}$, $\mathbf{c}' = \mathbf{c} - \mathbf{a}$, $\mathbf{d}' = \mathbf{d} - \mathbf{a}$.
 - (b) Construct the orthonormal frame $\mathbf{e}_1 = \frac{\mathbf{b}'}{\|\mathbf{b}'\|}$, $\mathbf{e}_2 = \frac{\mathbf{v}_2}{\|\mathbf{v}_2\|}$, where $\mathbf{v}_2 = \mathbf{c}' - (\mathbf{c}' \cdot \mathbf{e}_1)\mathbf{e}_1$ and $\mathbf{e}_3 = \mathbf{e}_1 \times \mathbf{e}_2$.
 - (c) Rotate the tetrahedron using $\mathbf{b}'' = R\mathbf{b}'$, $\mathbf{c}'' = R\mathbf{c}'$, $\mathbf{d}'' = R\mathbf{d}'$, where $R = \begin{bmatrix} \mathbf{e}_1^\top \\ \mathbf{e}_2^\top \\ \mathbf{e}_3^\top \end{bmatrix}$.
 - (d) Scale the tetrahedron by defining $\mathbf{b}''' = \frac{\mathbf{b}''}{\|\mathbf{b}''\|}$, $\mathbf{c}''' = \frac{\mathbf{c}''}{\|\mathbf{b}''\|}$, $\mathbf{d}''' = \frac{\mathbf{d}''}{\|\mathbf{b}''\|}$.

The coordinates of C are thus of the form $C = (c_1''', c_2''', 0)$. This corresponds to a point in the space of triangles $z = c_1''' + ic_2''' \in \mathcal{B}$.

3. **Placement of the fourth vertex.** After step 2. The coordinates of D are (d_1''', d_2''', d_3''') . To make sure that the point D ends up in the upper half-space, reflect if needed the third component to the upper half-space. In practice, $\mathbf{d}''''' = (d_1''', d_2''', |d_3'''|)$. Since the tetrahedron τ is non-degenerate, we get $d_3''' > 0$. This corresponds to a point $(w, t) \in \mathcal{V}(z)$, with $w := d_1''' + d_2'''i$ and $t = d_3'''$.

The resulting configuration $(z, (w, t)) \in \mathcal{T}$ defines the normalized form of the tetrahedron T .

Theorem 2.1. *The normalization map*

$$\begin{aligned} N : \mathcal{S} &\longrightarrow \mathcal{T} \\ T &\longmapsto \tau = (z, (w, t)) \end{aligned}$$

is surjective and constant on similarity classes. Moreover, for two tetrahedra T_1 and T_2 that are not shape similar, $T_1 \not\sim T_2$, then $N(T_1) \neq N(T_2)$.

Proof. By definition of the normalization procedure, any element $T \in \mathcal{S}$ is sent to \mathcal{T} , proving the surjectivity of N . When the longest canonical face is uniquely defined by step 1 of the normalization procedure, it follows that two shape similar tetrahedra will be mapped to the same element of \mathcal{T} .

The only case that need some care is when step 1 is still ambiguous because either two or more faces are similar or when the canonical face is isosceles with the two equal edges being the longest. In both cases, either step 1 and 2 in the normalization procedure lead to the same representation, or they lead to the vertex D being map either to the upper half-space, or to the lower half-space. Step 3 of the normalization procedure ensures that the choice of the canonical face is arbitrary and that the normalized form $N(T)$ is the same.

Finally, since two elements $\tau_1 \neq \tau_2$ of \mathcal{T} are not shape similar, it follows that two tetrahedra $T_1 \not\sim T_2$ will be mapped to different elements of \mathcal{T} , since shape similarity is preserved by the normalization map N . \square

Example 2.1. Let us consider the space-filling Sommerville tetrahedron [17] with vertices $(-1, 0, 0)$, $(1, 0, 0)$, $(0, -1, 1)$, and $(0, 1, 1)$. Applying the normalization procedure to this tetrahedron leads to the normalized representation $\tau^S := \left(\frac{1}{2} + \frac{\sqrt{2}}{2}i, \left(\frac{1}{2} + 0i, \frac{\sqrt{2}}{2}\right)\right)$.

Example 2.2. Let us consider the path tetrahedron with vertices $(0, 0, 0)$, $(1, 0, 0)$, $(1, 1, 0)$, and $(1, 1, 1)$. Applying the normalization procedure to this tetrahedron leads to the normalized representation $\tau^P := \left(\frac{1}{3} + \frac{\sqrt{2}}{3}i, \left(\frac{2}{3} + \frac{\sqrt{2}}{6}i, \frac{\sqrt{6}}{6}\right)\right)$.

Compared to the normalization procedure based on the square of edge lengths [14, 15], our normalization procedure yields an exact 5-dimensional representation of tetrahedra. In the rest of this paper, the normalization procedure will be carried out symbolically using the SymPy package [18] to avoid numerical inaccuracies and ensure the correct identification of similarity classes mirroring the integer-based strategy used in [14, 15].

Remark 2.2. It is possible to modify our methodology to resemble that of [14] by changing the base face used in the normalization procedure. In [14], the canonical face is defined by the longest edge, the longest adjacent edge to the longest. Ties are resolved by choosing the face with the longest edge closing the face. The difference in choices of canonical faces used during LEB refinements can lead to orbits of different lengths. However, both strategies are, obviously, still in the general framework of the LEB strategy.

2.3 LEB in the space of normalized tetrahedra

Let $T \in \mathcal{S}$ be a non-degenerate tetrahedron, $N(T) = (z, (w, t))$ its normalization and $\hat{T} = ABCD \in \mathcal{S}$ the corresponding canonical tetrahedron with vertices $A = (0, 0, 0)$, $B = (1, 0, 0)$, $C = (z_1, z_2, 0)$ and $D = (w_1, w_2, t)$. Under the LEB refinement, the tetrahedron \hat{T} is bisected by the plane passing through the midpoint M of its longest edge AB and the opposite vertices C and D . Since the longest edge of \hat{T} is AB , we define the vertex $M = (0.5, 0, 0)$ at the mid-point of AB . The left and right sub-tetrahedra T_L and T_R of \hat{T} are defined then as $T_L = AMCD$ and $T_R = MBCD$.

Definition 2.8. Let $T \in \mathcal{S}$ be a non-degenerate tetrahedron and $\tau = N(T)$ its normalized representation. The left and right maps associated to the LEB process are defined as the following:

$$\begin{aligned} \Phi_{L,R} : \mathcal{T} &\longrightarrow \mathcal{T} \\ \tau &\longmapsto \tau_{L,R} = N(T_{L,R}), \end{aligned}$$

respectively.

Remark 2.3. The maps Φ_L and Φ_R can be explicitly defined as functions of τ in a similar manner to what is done in [1, 2], but we are not doing it here. To do it, we would need to write down a formula for each of the 24 possible vertex orderings defined in step 1 of the normalization process for both the left and the right map, leading to 48 different expressions. In addition, we should specify conditions under which each transformation applies.

Definition 2.9. A region $\Omega \subset \mathcal{T}$ is called a closed region for LEB if for all $\tau \in \Omega$, we have $\Phi_L(\tau) \in \Omega$ and $\Phi_R(\tau) \in \Omega$.

Remark 2.4. By definition of $\Phi_{L,R}$, \mathcal{T} is a closed region for LEB.

Definition 2.10. Let $\tau \in \mathcal{T}$. We define $\Gamma_\tau^{(0)} = \{\tau\}$, and $\Gamma_\tau^{(n+1)} = \Phi_L(\Gamma_\tau^{(n)}) \cup \Phi_R(\Gamma_\tau^{(n)})$ for $n \geq 0$. The orbit of τ is defined then as the set $\Gamma_\tau := \bigcup_{n \geq 0} \Gamma_\tau^{(n)}$.

For any $\tau \in \mathcal{T}$, its orbit Γ_τ is closed by definition. In the rest of this paper, we will study the orbits of some specific tetrahedra.

3 On orbits produced by the LEB refinement algorithms

In this section, we study the orbits of various (normalized) tetrahedra under the LEB refinement algorithm. We will show that some tetrahedra have very short orbits. As pointed out already in [13], the orbit of the Sommerville tetrahedron contains only four elements and the orbit of the path tetrahedron contains only three elements. This has also been noted by Trujillo-Pino *et al.* [15], where the orbit of the Sommerville tetrahedron has been studied using the squared edge length normalization procedure. Here, we prove that the orbit of the path tetrahedron is actually included in that of the Sommerville tetrahedron. In addition, we show that small perturbations of elements from these orbits still lead to finite but longer orbits. The we use our algorithm to study nearly regular tetrahedra and compare it to previous results [14]. Finally, we study four cases that do not seem to have finite orbits.

3.1 The case of the Sommerville tetrahedron

The space-filling Sommerville tetrahedron [17] plays a special role in the LEB refinement algorithm as well as in numerical analysis in general [19]. The following result holds.

Theorem 3.1. *The orbit of the Sommerville tetrahedron contains four elements. Its orbit is attracted into a cycle of length three including the path tetrahedron. Hence, the orbit of the path tetrahedron contains exactly three elements.*

Proof. As mentioned in Example 2.1, the normalized representation of the Sommerville tetrahedron is $\tau^S := \left(\frac{1}{2} + \frac{\sqrt{2}i}{2}, \left(\frac{1}{2} + 0i, \frac{\sqrt{2}}{2} \right) \right)$. Applying the left and right maps to τ^S and iterating, we find that

- $\Phi_L(\tau^S) = \Phi_R(\tau^S) = \left(\frac{1}{2} + \frac{i}{2}, \left(\frac{1}{2} + \frac{i}{2}, \frac{1}{2} \right) \right) =: \tau^H$,
- $\Phi_L(\tau_1) = \Phi_R(\tau_1) = \left(\frac{1}{3} + \frac{\sqrt{2}i}{3}, \left(\frac{2}{3} + \frac{\sqrt{2}i}{6}, \frac{\sqrt{6}}{6} \right) \right) =: \tau^P$,
- $\Phi_L(\tau^P) = \Phi_R(\tau^P) = \left(\frac{1}{2} + \frac{\sqrt{2}i}{4}, \left(\frac{1}{2} + 0i, \frac{1}{2} \right) \right) =: \tau^Q$,
- $\Phi_L(\tau_2) = \Phi_R(\tau_2) = \tau^H$.

The proof is illustrated in Figure 3. □

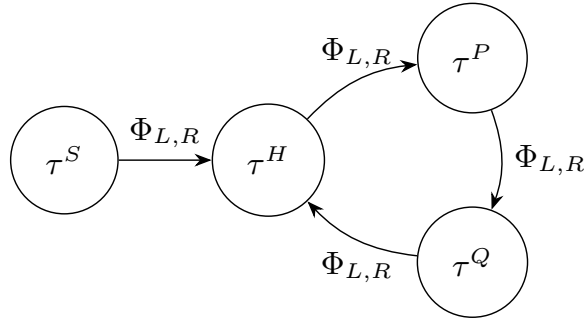


Figure 3: The orbit of the Sommerville tetrahedron.

Remark 3.1. *In order to simplify further discussion, we denote each element in the orbit of the Sommerville tetrahedron τ^S as marked in Figure 3. We use the denotation τ^H for the first element because all its non-trivial components are equal to $\frac{1}{2}$ and H stands for halves. τ^P is the path tetrahedron and τ^Q is its image under $\Phi_{L,R}$.*

Theorem 3.1 confirms the result of [13] and [15] for the number of shapes in the orbits of these two specific tetrahedra. Visualization of the orbit of the Sommerville tetrahedron is presented in Figure 4.

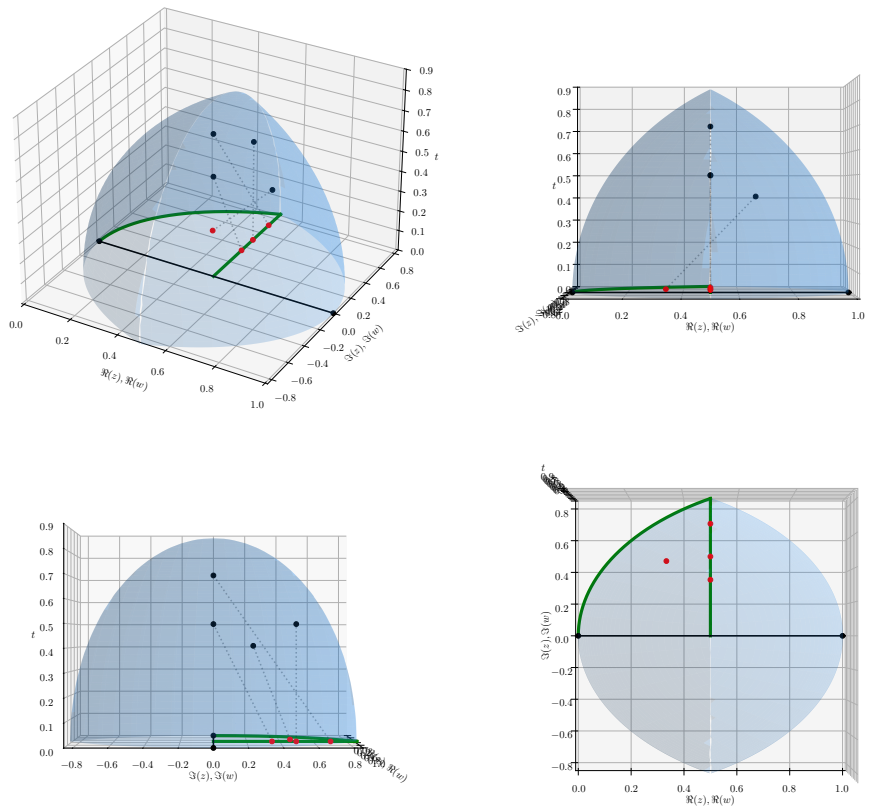


Figure 4: Visualization of the orbit of the Sommerville tetrahedron. The first three panels show different views of the same results. The bottom right panel shows only the positions of the base vertices.

3.2 Orbits of small perturbations of the Sommerville and path tetrahedra

In [2], the idea for constructing the proof of regularity of the bisection process essentially consists of introducing the hyperbolic metric and showing that some regions of the canonical space of triangles are closed. In order to test whether a certain neighborhood of the orbit of the Sommerville tetrahedron is closed, we make small perturbations of the Sommerville tetrahedron and of some elements from its orbit and monitor the resulting orbits.

Example 3.1. *We apply LEB refinements to the tetrahedron with vertices $(-1, 0, 0)$, $(1, 0, 0)$, $(0, -1, 1)$, and $(0, 1, \frac{11}{10})$, which normalizes to $\tilde{\tau}^S = \left(\frac{190}{401} + \frac{10\sqrt{842}}{401}i, \left(\frac{190}{401} + \frac{200\sqrt{842}}{168821}i, \frac{210\sqrt{337642}}{168821} \right) \right)$. How the different tetrahedra in the resulting finite orbit (of length 25) map onto each other is illustrated in Figure 5. The orbit of this tetrahedron is displayed in Figure 6.*

Consider the perturbation $\tilde{\tau}^S$ of the Sommerville tetrahedron defined in Example 3.1. This size of this perturbation is $d_{\mathcal{T}}(\tau^S, \tilde{\tau}^S) = 7.75 \cdot 10^{-2}$ and its orbit is shown in Figure 5. We observe that the orbit of $\tilde{\tau}^S$ gets attracted in a sub-orbit of length 24 composed of three clusters. Similarly to what happens for τ^S , the orbit of $\tilde{\tau}^S$ gets attracted into three clusters corresponding to the other elements of the orbit of τ^S . Using the notation introduced in Proposition 3.1 and discussed in Remark 3.1, the three clusters are referred to as $c^H = \{\tau_2, \dots, \tau_{11}\}$, $c^P = \{\tau_{12}, \dots, \tau_{17}\}$, and $c^Q = \{\tau_{18}, \dots, \tau_{25}\}$, where the elements are defined in Figure 5. For each of these clusters, we can compute the average distance of the elements to reference shapes defining the clusters. For example, if we consider c^H , the average distance to τ^H is given by

$$\overline{d_{\mathcal{T}}}(c^H, \tau^H) := \frac{1}{|c^H|} \sum_{\tau \in c^H} d_{\mathcal{T}}(\tau, \tau^H)$$

and similarly for other clusters. We obtain $\overline{d_{\mathcal{T}}}(c^H, \tau^H) = 8.41 \cdot 10^{-2}$, $\overline{d_{\mathcal{T}}}(c^P, \tau^P) = 8.00 \cdot 10^{-2}$ and $\overline{d_{\mathcal{T}}}(c^Q, \tau^Q) = 7.43 \cdot 10^{-2}$, which are of similar size to the original perturbation.

Remark 3.2. *In Example 3.1, we obtained orbits of lengths 24 and 25. These lengths were not reported in Padrón et al. [20], where they identified finite orbits of length $n \in \{4, 8, 9, 13, 21, 37\}$ and the orbit of length 4 is that of τ^S . However, the normalized tetrahedron $\tilde{\tau}^S \in R_1^+$ (the R_1^+ family is defined in Definition 2 of [20]), the family of tetrahedra to which their result applies. We believe that the discrepancy originates in the different normalization procedures used in both approaches discussed in Remark 2.2.*

To test whether shorter orbits are possible as well, we modified the element $\tau^H = \left(\frac{1}{2} + \frac{1}{2}i, \left(\frac{1}{2} + \frac{1}{2}i, \frac{1}{2} \right) \right)$ from the orbit of the Sommerville tetrahedron.

Conjecture 3.1. *Let $\tau^H = (z^H, (w^H, t^H) = \left(\frac{1}{2} + \frac{1}{2}i, \left(\frac{1}{2} + \frac{1}{2}i, \frac{1}{2} \right) \right)$. When modifying τ^H component-wise, we can obtain orbits of lengths $n \in \{7, 8, 21, 22, 23, 24, 25, 26\}$. More precisely, we have*

- For $\tilde{\tau}_{1,\alpha}^H = \left(\frac{1}{2} - \alpha + \frac{1}{2}i, \left(\frac{1}{2} + \frac{1}{2}i, \frac{1}{2} \right) \right)$, $\alpha \in]0, \frac{1}{10}]$, the orbit $\Gamma_{\tilde{\tau}_{1,\alpha}^H}$ has length 21.
- For $\tilde{\tau}_{2,\alpha}^H = \left(\frac{1}{2} + \left(\frac{1}{2} + \alpha \right)i, \left(\frac{1}{2} + \frac{1}{2}i, \frac{1}{2} \right) \right)$, $\alpha \in [-\frac{3}{50}, \frac{1}{10}]$, $\alpha \neq 0$, the orbit $\Gamma_{\tilde{\tau}_{2,\alpha}^H}$ has length between 22 or 24.
- For $\tilde{\tau}_{3,\alpha}^H = \left(\frac{1}{2} + \frac{1}{2}i, \left(\frac{1}{2} - \alpha + \frac{1}{2}i, \frac{1}{2} \right) \right)$, $\alpha \in]0, \frac{2}{10}]$, the orbit $\Gamma_{\tilde{\tau}_{3,\alpha}^H}$ has length 23, 24 or 26.
- For $\tilde{\tau}_{4,\alpha}^H = \left(\frac{1}{2} + \frac{1}{2}i, \left(\frac{1}{2} + \left(\frac{1}{2} + \alpha \right)i, \frac{1}{2} \right) \right)$, $\alpha \in [-\frac{2}{10}, \frac{2}{10}]$, $\alpha \neq 0$, the orbit $\Gamma_{\tilde{\tau}_{4,\alpha}^H}$ has length 23, 24, 25, or 26.
- For $\tilde{\tau}_{5,\alpha}^H = \left(\frac{1}{2} + \frac{1}{2}i, \left(\frac{1}{2} + \frac{1}{2}i, \frac{1}{2} + \alpha \right) \right)$, $\alpha \in [-\frac{9}{100}, \frac{2}{10}]$, $\alpha \neq 0$, the orbit $\Gamma_{\tilde{\tau}_{5,\alpha}^H}$ has length 7 or 8.

ID	Normalization
τ_1	$\left(\frac{190}{401} + \frac{10\sqrt{842}}{401}i, \left(\frac{190}{401} + \frac{200\sqrt{842}}{168821}i, \frac{210\sqrt{337642}}{168821}\right)\right)$
τ_2	$\left(\frac{1}{2} + \frac{21}{40}i, \left(\frac{1}{2} + \frac{1}{2}i, \frac{1}{2}\right)\right)$
τ_3	$\left(\frac{1}{2} + \frac{10}{21}i, \left(\frac{10}{21} + \frac{10}{21}i, \frac{10}{21}\right)\right)$
τ_4	$\left(\frac{1}{2} + \frac{\sqrt{401}}{40}i, \left(\frac{1}{2} + \frac{211\sqrt{401}}{8020}i, \frac{21\sqrt{401}}{802}\right)\right)$
τ_5	$\left(\frac{1}{2} + \frac{10}{21}i, \left(\frac{11}{21} + \frac{10}{21}i, \frac{10}{21}\right)\right)$
τ_6	$\left(\frac{1}{2} + \frac{10\sqrt{401}}{401}i, \left(\frac{211}{401} + \frac{10\sqrt{401}}{401}i, \frac{210}{401}\right)\right)$
τ_7	$\left(\frac{190}{401} + \frac{210}{401}i, \left(\frac{190}{401} + \frac{210}{401}i, \frac{10\sqrt{401}}{401}\right)\right)$
τ_8	$\left(\frac{10}{21} + \frac{10}{21}i, \left(\frac{10}{21} + \frac{10}{21}i, \frac{10}{21}\right)\right)$
τ_9	$\left(\frac{1}{2} + \frac{\sqrt{401}}{40}i, \left(\frac{1}{2} + \frac{19\sqrt{401}}{802}i, \frac{21\sqrt{401}}{802}\right)\right)$
τ_{10}	$\left(\frac{1}{2} + \frac{10\sqrt{401}}{401}i, \left(\frac{190}{401} + \frac{10\sqrt{401}}{401}i, \frac{210}{401}\right)\right)$
τ_{11}	$\left(\frac{1}{2} + \frac{21}{40}i, \left(\frac{1}{2} + \frac{11}{20}i, \frac{1}{2}\right)\right)$
τ_{12}	$\left(\frac{1}{3} + \frac{\sqrt{2}}{3}i, \left(\frac{13}{20} + \frac{7\sqrt{2}}{40}i, \frac{7\sqrt{6}}{40}\right)\right)$
τ_{13}	$\left(\frac{1}{3} + \frac{\sqrt{2}}{3}i, \left(\frac{41}{60} + \frac{19\sqrt{2}}{120}i, \frac{7\sqrt{6}}{40}\right)\right)$

ID	Normalization
τ_{14}	$\left(\frac{19}{60} + \frac{\sqrt{842}}{60}i, \left(\frac{13}{20} + \frac{77\sqrt{842}}{8420}i, \frac{7\sqrt{2526}}{842}\right)\right)$
τ_{15}	$\left(\frac{100}{321} + \frac{10\sqrt{221}}{321}i, \left(\frac{431}{642} + \frac{1055\sqrt{221}}{70941}i, \frac{35\sqrt{70941}}{23647}\right)\right)$
τ_{16}	$\left(\frac{100}{321} + \frac{10\sqrt{221}}{321}i, \left(\frac{137}{214} + \frac{385\sqrt{221}}{23647}i, \frac{35\sqrt{70941}}{23647}\right)\right)$
τ_{17}	$\left(\frac{211}{642} + \frac{5\sqrt{842}}{321}i, \left(\frac{137}{214} + \frac{350\sqrt{842}}{45047}i, \frac{35\sqrt{270282}}{45047}\right)\right)$
τ_{18}	$\left(\frac{410}{841} + \frac{10\sqrt{842}}{841}i, \left(\frac{441}{841} - \frac{210\sqrt{842}}{354061}i, \frac{210\sqrt{842}}{12209}\right)\right)$
τ_{19}	$\left(\frac{130}{267} + \frac{70\sqrt{2}}{267}i, \left(\frac{401}{801} - \frac{10\sqrt{2}}{801}i, \frac{10\sqrt{178}}{267}\right)\right)$
τ_{20}	$\left(\frac{410}{841} + \frac{10\sqrt{842}}{841}i, \left(\frac{400}{841} + \frac{210\sqrt{842}}{354061}i, \frac{210\sqrt{842}}{12209}\right)\right)$
τ_{21}	$\left(\frac{1}{2} + \frac{\sqrt{2}}{4}i, \left(\frac{19}{40} + 0i, \frac{21}{40}\right)\right)$
τ_{22}	$\left(\frac{1}{2} + \frac{\sqrt{2}}{4}i, \left(\frac{21}{40} + 0i, \frac{21}{40}\right)\right)$
τ_{23}	$\left(\frac{130}{267} + \frac{70\sqrt{2}}{267}i, \left(\frac{400}{801} + \frac{10\sqrt{2}}{801}i, \frac{10\sqrt{178}}{267}\right)\right)$
τ_{24}	$\left(\frac{1}{2} + \frac{5\sqrt{221}}{221}i, \left(\frac{231}{442} + 0i, \frac{105}{221}\right)\right)$
τ_{25}	$\left(\frac{1}{2} + \frac{5\sqrt{221}}{221}i, \left(\frac{211}{442} + 0i, \frac{105}{221}\right)\right)$

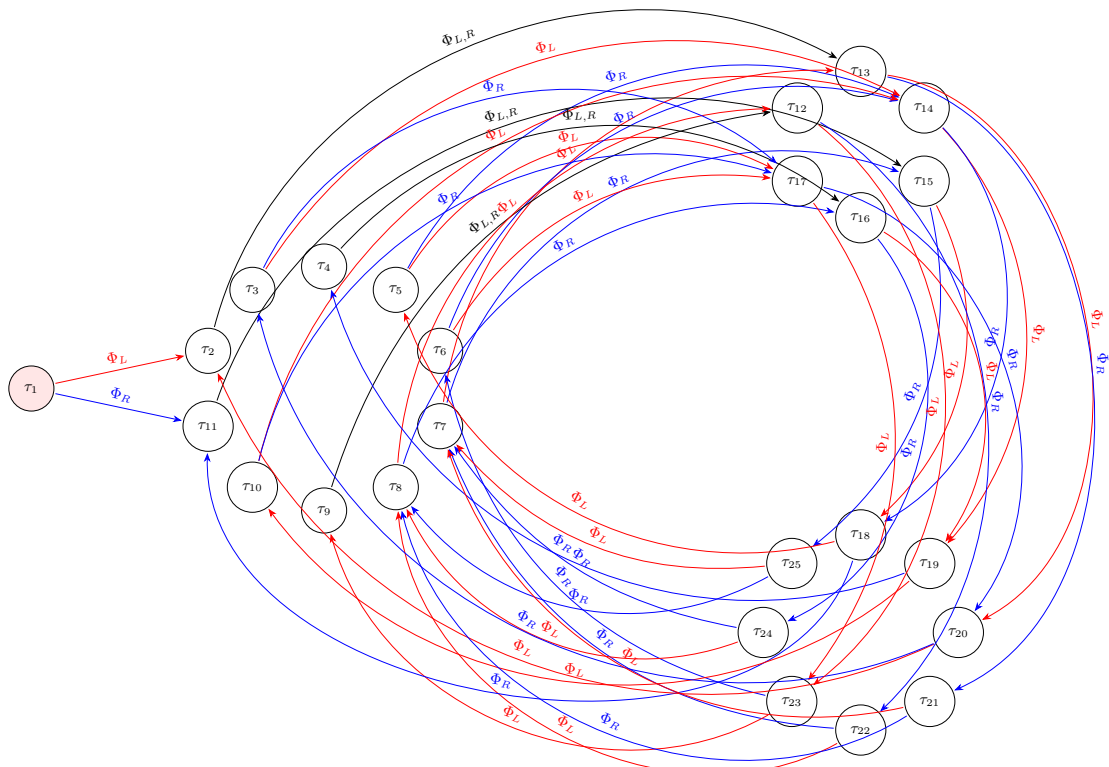


Figure 5: The results of Example 3.1 illustrated. Graph shows how the normalized tetrahedra listed in the tables at the top and marked by nodes in the diagram map onto each other under the action of Φ_L (red) and Φ_R (blue). All the tetrahedra involved are grouped according to how they cluster. The red node τ_1 corresponds to the modification of the Sommerville tetrahedron, and it has no incoming edges.

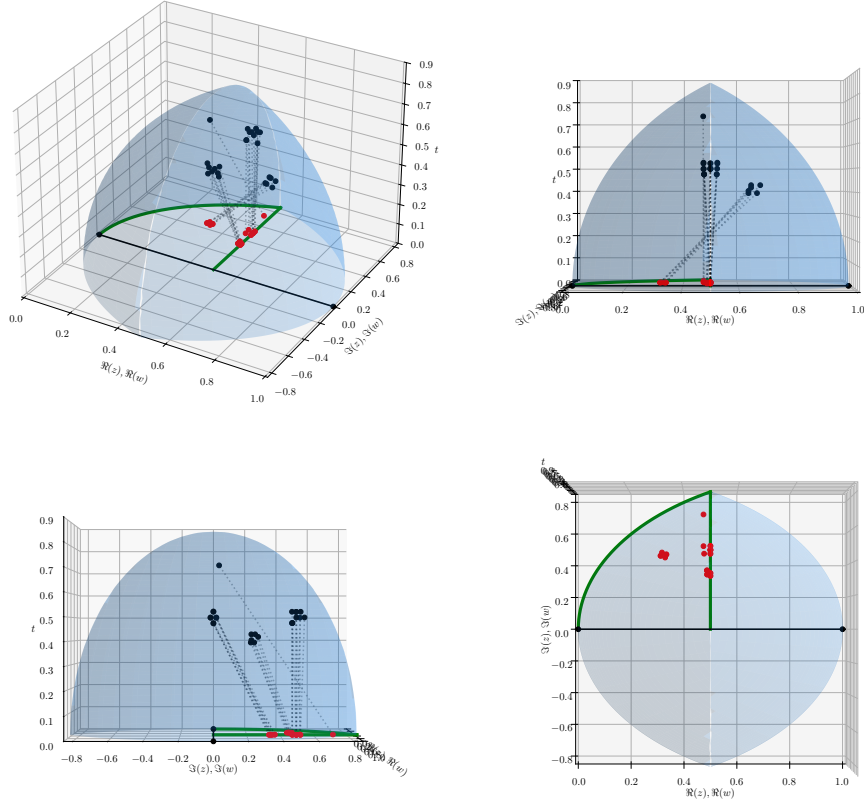


Figure 6: Orbit of the perturbed Sommerville tetrahedra with vertices $(-1, 0, 0)$, $(1, 0, 0)$, $(0, -1, 1)$, and $(0, 1, \frac{11}{10})$. The bottom right panel shows only the positions of the base vertices.

We have not been able to prove Conjecture 3.1, but we have strong evidence that it holds true. To show that we performed experiments in which the value of α was systematically changed by steps of $\frac{1}{100}$ (we use \dots , when all the $\frac{1}{100}$ steps between limits lead to the same length of the orbit) and recorded the length of the orbit. We obtained the following results:

- For $\alpha \in \{\frac{1}{100}, \dots, \frac{10}{100}\}$, the orbit $\Gamma_{\tilde{\tau}_{1,\alpha}^H}$ has length 21 and the orbit $\Gamma_{\tilde{\tau}_{2,\alpha}^H}$ has length 24.
- For $\alpha \in \{-\frac{1}{100}, \dots, -\frac{3}{100}\}$, the orbit $\Gamma_{\tilde{\tau}_{2,\alpha}^H}$ has length 22.
- For $\alpha \in \{-\frac{4}{100}, \dots, -\frac{6}{100}\}$, the orbit $\Gamma_{\tilde{\tau}_{2,\alpha}^H}$ has length 23.
- For $\alpha \in \{\frac{1}{100}, \frac{3}{100}, \frac{5}{100}, \dots, \frac{9}{100}, \frac{11}{100}, \frac{12}{100}, \frac{15}{100}, \dots, \frac{20}{100}\}$, the orbits $\Gamma_{\tilde{\tau}_{3,\alpha}^H}$ and $\Gamma_{\tilde{\tau}_{4,\alpha}^H}$ have length 26.
- For $\alpha \in \{\frac{2}{100}, \frac{4}{100}, \frac{14}{100}\}$, the orbits $\Gamma_{\tilde{\tau}_{3,\alpha}^H}$ and $\Gamma_{\tilde{\tau}_{4,\alpha}^H}$ have length 23.
- For $\alpha \in \{\frac{10}{100}, \frac{13}{100}\}$, the orbits $\Gamma_{\tilde{\tau}_{3,\alpha}^H}$ and $\Gamma_{\tilde{\tau}_{4,\alpha}^H}$ have length 24.
- For $\alpha \in \{-\frac{1}{100}, -\frac{3}{100}, -\frac{5}{100}, \dots, -\frac{7}{100}, -\frac{9}{100}, -\frac{11}{100}, -\frac{12}{100}, -\frac{15}{100}, \dots, \frac{19}{100}\}$, the orbit $\Gamma_{\tilde{\tau}_{4,\alpha}^H}$ has length 23.
- For $\alpha = \frac{2}{10}$, the orbit $\Gamma_{\tilde{\tau}_{4,\alpha}^H}$ has length 25.
- For $\alpha \in \{\frac{1}{100}, \dots, \frac{20}{100}\}$, the orbit $\Gamma_{\tilde{\tau}_{5,\alpha}^H}$ has length 8.

ID	Normalization
τ_1	$(\frac{1}{2} + \frac{11}{20}i, (\frac{1}{2} + \frac{11}{20}i, \frac{1}{2}))$
τ_2	$(\frac{1}{2} + \frac{1}{2}i, (\frac{1}{2} + \frac{1}{2}i, \frac{11}{20}))$
τ_3	$(\frac{1}{2} + \frac{5}{11}i, (\frac{1}{2} + \frac{5}{11}i, \frac{5}{11}))$
τ_4	$(\frac{100}{321} + \frac{10\sqrt{221}}{321}i, (\frac{200}{321} + \frac{1210\sqrt{221}}{70941}i, \frac{110\sqrt{70941}}{70941}))$
τ_5	$(\frac{100}{321} + \frac{10\sqrt{221}}{321}i, (\frac{221}{321} + \frac{1000\sqrt{221}}{70941}i, \frac{110\sqrt{70941}}{70941}))$
τ_6	$(\frac{1}{2} + \frac{11\sqrt{2}}{40}i, (\frac{1}{2} + 0i, \frac{1}{2}))$
τ_7	$(\frac{1}{2} + \frac{5\sqrt{221}}{221}i, (\frac{100}{221} + 0i, \frac{110}{221}))$
τ_8	$(\frac{1}{2} + \frac{5\sqrt{221}}{221}i, (\frac{121}{221} + 0i, \frac{110}{221}))$

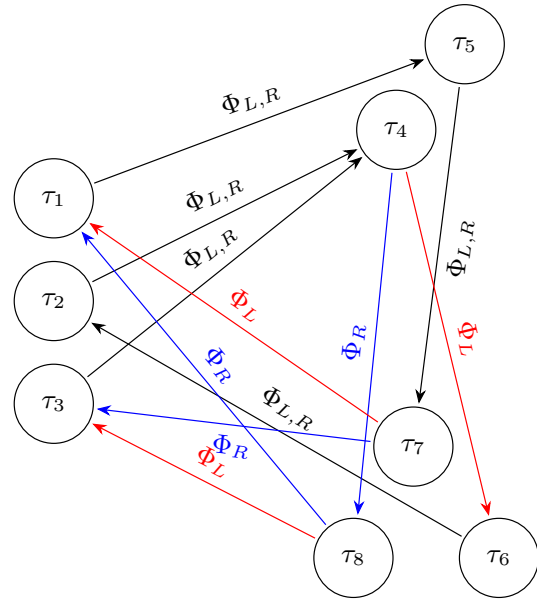


Figure 7: An example of an orbit of length 8. Left: list of tetrahedra in the orbit. Right: graph of how they map onto each other.

- For $\alpha \in \{-\frac{1}{100}, -\frac{3}{100}, -\frac{5}{100}, \dots, -\frac{9}{100}\}$, the orbit $\Gamma_{\tilde{\tau}_{5,\alpha}^H}$ has length 8.
- For $\alpha \in \{-\frac{2}{100}, -\frac{34}{100}\}$, the orbit $\Gamma_{\tilde{\tau}_{5,\alpha}^H}$ has length 7.

Outside of the intervals specified in Conjecture 3.1, the orbits seem to diverge. For example, we observe that the length of $\Gamma_{\tilde{\tau}_{2,\frac{11}{100}}^H}$ already contains 382 shapes after 20 iterations.

Example 3.2. We modify the tetrahedron with normalization $\tau^H = (\frac{1}{2} + \frac{1}{2}i, (\frac{1}{2} + \frac{1}{2}i, \frac{1}{2}))$ from the orbit of the Sommerville tetrahedron to $\tilde{\tau}_{5,\frac{1}{20}}^H = (\frac{1}{2} + \frac{1}{2}i, (\frac{1}{2} + \frac{1}{2}i, \frac{11}{20}))$. This tetrahedron has an orbit of length 8 containing the tetrahedra listed in Figure 7 and visualized in Figure 8.

Example 3.2 illustrates the orbit of $\tilde{\tau}_{5,\frac{1}{20}}^H$, which has an orbit of length 8 as predicted by Conjecture 3.1. This is a perturbation of size $d\tau(\tilde{\tau}_{5,\frac{1}{20}}^H, \tau^H) = 9.53 \cdot 10^{-2}$. In Figure 7, the 8 shapes in the orbit of $\tilde{\tau}_{5,\frac{1}{20}}^H$ are listed in the table on the left, and the graph of how they map onto each other is displayed on the right. A visualization of the orbit is provided in Figure 8. We clearly identify three clusters of normalized tetrahedra corresponding to τ^H , τ^P and τ^Q denoted as before by $c_{5,\frac{1}{20}}^H = \{\tau_1, \tau_2, \tau_3\}$, $c_{5,\frac{1}{20}}^P = \{\tau_4, \tau_5\}$, and $c_{5,\frac{1}{20}}^Q = \{\tau_6, \tau_7, \tau_8\}$. The average distances to the reference elements are $\overline{d\tau}(c_{5,\frac{1}{20}}^H, \tau^H) = 1.33 \cdot 10^{-1}$, $\overline{d\tau}(c_{5,\frac{1}{20}}^P, \tau^P) = 1.12 \cdot 10^{-1}$, and $\overline{d\tau}(c_{5,\frac{1}{20}}^Q, \tau^Q) = 1.03 \cdot 10^{-1}$.

Remark 3.3. Conjecture 3.1 only concerns modifications of a single component of τ^H . When modifying more components at once, we can obtain orbits of other lengths. For example, the tetrahedron $\tilde{\tau}_1 = (\frac{1}{2} + \frac{\sqrt{442}}{40}i, (\frac{1}{2} + \frac{5\sqrt{442}}{221}i, \frac{11\sqrt{442}}{442}))$ has an orbit of length 13 that can be reached from the modification of the Sommerville tetrahedron $\tilde{\tau}_1^S = (\frac{100}{221} + \frac{5\sqrt{926}}{221}i, (\frac{100}{221} + \frac{105\sqrt{926}}{102323}i, \frac{220\sqrt{102323}}{102323}))$ which has an orbit of length 14. Furthermore, the tetrahedron $\tilde{\tau}_2 = (\frac{1}{2} + \frac{1}{2}i, (\frac{53}{100} + \frac{49}{100}i, \frac{3}{5}))$ has an orbit of length 44.

The results obtained in this section show that small perturbations of τ^S or of τ^H , may lead to finite orbits of various lengths. So far, we have shown orbits of lengths $n \in \{3, 4, 7, 8, 13, 14, 21, 22, 23, 24, 25, 26, 44\}$. In the next section, we look at small perturbations of the regular tetrahedron, since this family of tetrahedra has been extensively studied in [14, 15].

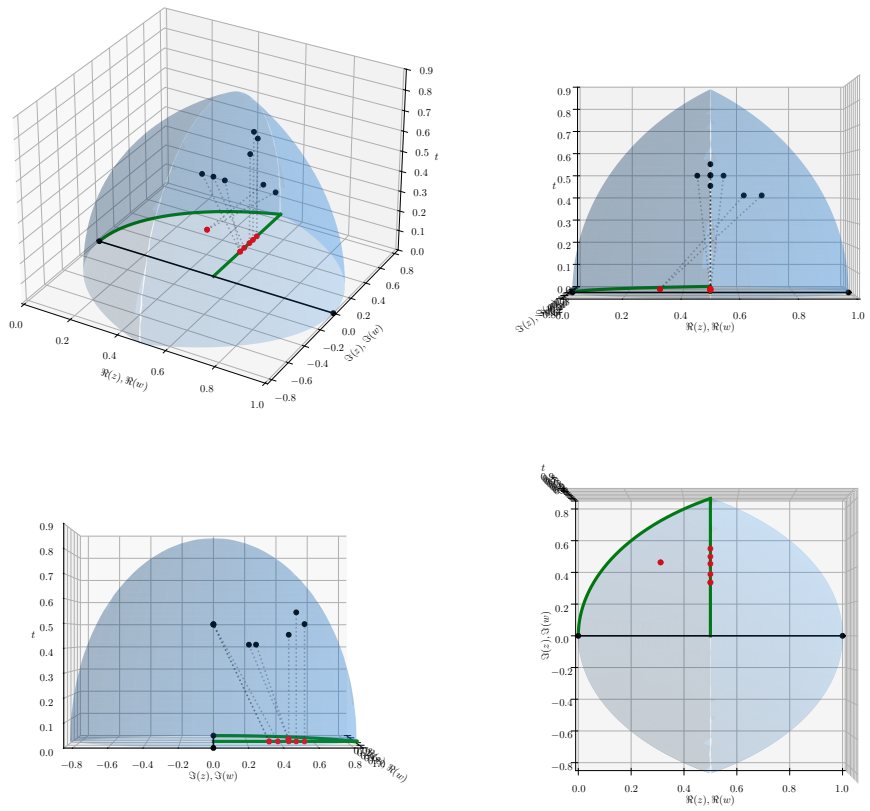


Figure 8: Visualization of the orbit of length 8 from Figure 7. The bottom right panel shows only the positions of the base vertices.

3.3 Orbits of small perturbations of the regular tetrahedron

In [14, 15, 20], a family of nearly equilateral tetrahedra is studied and it is shown that at most 37 similarity classes can be produced. This limit was mentioned by Adler [21] already in 1983, but without any proof. Here we apply our normalization procedure to six tetrahedra listed in [14] to test whether our normalization procedure and our implementation the LEB algorithm reproduces the results mentioned above. Note that the orbit of length 44 mentioned in Remark 3.3 does not contradict the upper limit of 37 similarity classes, since the tetrahedron taken as an example does not belong to the family of tetrahedra studied in [14, 15, 20].

Table 1: List of the tetrahedra used in [14] and the length of their orbits.

ID	Vertex coordinates	Normalized form	Orbit length
T1	$(0, 0, 0), (\sqrt{22}, 0, 0), \left(\frac{5\sqrt{22}}{11}, \frac{\sqrt{1507}}{11}, 0\right), \left(\frac{21\sqrt{22}}{44}, \frac{49\sqrt{1507}}{3014}, \frac{\sqrt{3480622}}{548}\right)$	$\left(\frac{5}{11} + \frac{\sqrt{274}}{22}i, \left(\frac{21}{44} + \frac{49\sqrt{274}}{6028}i, \frac{\sqrt{19143421}}{6028}\right)\right)$	39
T2	$(0, 0, 0), (\sqrt{21}, 0, 0), \left(\frac{3\sqrt{21}}{7}, \frac{\sqrt{595}}{7}, 0\right), \left(\frac{10\sqrt{21}}{21}, \frac{31\sqrt{595}}{1190}, \frac{\sqrt{3078105}}{510}\right)$	$\left(\frac{3}{7} + \frac{\sqrt{255}}{21}i, \left(\frac{10}{21} + \frac{31\sqrt{255}}{3570}i, \frac{\sqrt{7182245}}{3570}\right)\right)$	37
T3	$(0, 0, 0), (\sqrt{21}, 0, 0), \left(\frac{\sqrt{21}}{2}, \frac{\sqrt{47}}{2}, 0\right), \left(\frac{11\sqrt{21}}{21}, \frac{4\sqrt{47}}{47}, \frac{2\sqrt{2654043}}{987}\right)$	$\left(\frac{10}{21} + \frac{2\sqrt{59}}{21}i, \left(\frac{1}{2} + \frac{\sqrt{59}}{59}i, \frac{\sqrt{3331671}}{2478}\right)\right)$	43
T4	$(0, 0, 0), (\sqrt{41}, 0, 0), \left(\frac{20\sqrt{41}}{41}, \frac{\sqrt{47478}}{41}, 0\right), \left(\frac{21\sqrt{41}}{41}, \frac{53\sqrt{47478}}{7913}, \frac{\sqrt{935471}}{193}\right)$	$\left(\frac{20}{41} + \frac{\sqrt{1117}}{41}i, \left(\frac{21}{41} + \frac{318\sqrt{1117}}{45797}i, \frac{\sqrt{1331868354}}{45797}\right)\right)$	43
T5	$(0, 0, 0), (10, 0, 0), \left(\frac{99}{20}, \frac{\sqrt{28999}}{20}, 0\right), \left(\frac{101}{20}, \frac{9001\sqrt{28999}}{579980}, \frac{\sqrt{1870811}}{28999}\right)$	$\left(\frac{99}{200} + \frac{\sqrt{28599}}{200}i, \left(\frac{101}{200} + \frac{9001\sqrt{28599}}{5719800}i, \frac{\sqrt{53503323789}}{285990}\right)\right)$	43
T6	$(0, 0, 0), (10, 0, 0), \left(\frac{99}{20}, \frac{\sqrt{28999}}{20}, 0\right), \left(\frac{101}{20}, \frac{8801\sqrt{28999}}{579980}, \frac{\sqrt{1850713}}{28999}\right)$	$\left(\frac{99}{200} + \frac{\sqrt{28199}}{200}i, \left(\frac{101}{200} + \frac{8801\sqrt{28199}}{5639800}i, \frac{\sqrt{52188255887}}{281990}\right)\right)$	37

Theorem 3.2. *The six tetrahedra listed in Table 1 have finite orbits as listed in the table.*

Proof. This is shown by direct computation. For example, the normalized forms of the tetrahedra in the orbit of T1 are listed in Table 3. \square

Remark 3.4. *Theorem 3.2 shows that, contrarily to the conjecture by Adler [21] and studied in [15, 20], it is possible to obtain finite orbits longer than 37. We do recover, for T2 and T6, the orbit of length 37, but the other tetrahedra in Table 1 have longer orbits. We believe that the discrepancy comes from the different normalization used in our work from that one used in [15, 20], which, as pointed out in Remark 2.2 may lead to a different choices of the longest edge to be bisected and hence, may lead to orbits of different lengths. As a result, the proofs developed in [15, 20] are only valid for their normalization procedure and the implied choice of the edge to be bisected. In general, their result that the number of similarity classes of nearly equilateral tetrahedra being bounded by 37 does not seem to hold.*

An interesting question is how do these orbits look like, do they also cluster like the perturbations of τ^S and τ^H ? To answer this question, we provide a visualization of the orbit of T5 containing 43 shapes in Figure 9.

As can be seen from the figure, the orbit clearly shows clustering. The 43 shapes seem to be attracted to a sub-orbit of length 42 that clusters around 8 points in \mathcal{T} . This number of clusters is reminiscent of the result in [22] which states that the minimal number of similarity classes of the regular tetrahedron following the Branch-and-Bound algorithm is 8. Since the tetrahedron is nearly equilateral, some of the ambiguity of choosing the edge is eliminated, thus allowing the orbit to be attracted to a short orbit.

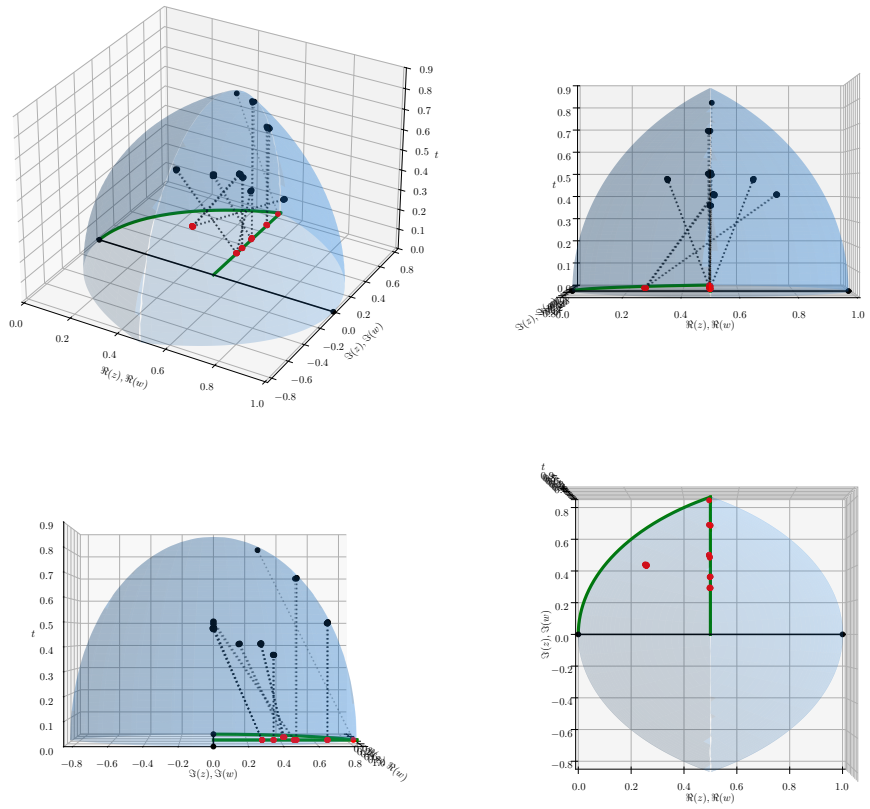


Figure 9: Orbit of the tetrahedron T5 from Table 1. The bottom right panel shows only the positions of the base vertices.

Remark 3.5. *The fact that the orbit never comes back to its starting point is valid for all tetrahedra listed in Table 1. This implies the existence of orbits of length $n \in \{36, 37, 38, 39, 42, 43\}$.*

Remark 3.6. *The attracting sub-orbit in the orbit of $T5$ does not overlap that of τ^P . These are two different attracting cycles.*

Theorem 3.3. *There exists finite orbits under LEB of lengths $n \in \{3, 4, 7, 8, 13, 14\} \cup \{21, \dots, 26\} \cup \{36, 37, 38, 39, 42, 43, 44\}$.*

Proof. This Theorem collects the results of Thm 3.1, Examples 3.1 and 3.2, of the illustration of Conjecture 3.1 and Remarks 3.3 and 3.5. \square

In the next section, we will show that the regular tetrahedron is not as well-behaved and that its orbit does not seem to be finite.

3.4 On the behaviour of LEB on general tetrahedra

We now discuss four cases of tetrahedra that do not seem to have finite orbits. We consider the regular tetrahedron, the cube corner tetrahedron and two nearly degenerate tetrahedra and iterate the LEB process for $n = 40$ iterations and record how many shapes appear in the resulting orbits, the minimal face and dihedral angles as well as their normalized volumes. In order to get a better interpretation of the volumes, we normalize the volume by the maximum possible volume of a normalized tetrahedron, i.e. the volume of the regular tetrahedron of edge length 1. This volume is given by $\frac{\sqrt{2}}{12}$. Hence, the volumes are reported in percent of the volume of the regular tetrahedron, see Table 2 and Figure 10.

Example 3.3. *The regular tetrahedron is given in normalized form as $\tau^R = \left(\frac{1}{2} + \frac{\sqrt{3}}{2}i, \left(\frac{1}{2} + \frac{\sqrt{3}}{6}i, \frac{\sqrt{6}}{3} \right) \right)$. Applying the LEB refinement process to this tetrahedron does not seem to lead to a finite orbit.*

Example 3.4. *The cube corner tetrahedron with vertices $(0, 0, 0), (1, 0, 0), (0, 1, 0)$ and $(0, 0, 1)$ is given in normalized form as $\tau^C = \left(\frac{1}{2} + \frac{1}{2}i, \left(\frac{1}{2} + \frac{1}{2}i, \frac{\sqrt{2}}{2} \right) \right)$. Applying the LEB refinement process to this tetrahedron does not seem to lead to a finite orbit.*

Example 3.5. *The wedge tetrahedron with vertices $(0, 0, 0), (1, 0, 0), (0, 1, 0)$ and $(0, 0, \frac{1}{10})$ is given in normalized form as $\tau^W = \left(\frac{1}{2} + \frac{1}{2}i, \left(\frac{1}{2} + \frac{1}{2}i, \frac{\sqrt{2}}{20} \right) \right)$. Applying the LEB refinement process to this tetrahedron does not seem to lead to a finite orbit.*

Example 3.6. *The needle tetrahedron also with vertices $(0, \frac{1}{10\sqrt{3}}, 0), (\frac{1}{20}, -\frac{1}{20\sqrt{3}}, 0), (-\frac{1}{20}, -\frac{1}{20\sqrt{3}}, 0)$ and $(0, 0, 1)$ (its base is an equilateral triangle in xy -plane with the edge lengths equal to 0.1) used in [13] is given in normalized form as $\tau^N = \left(\frac{3}{602} + \frac{\sqrt{3603}}{602}i, \left(\frac{3}{602} + \frac{599\sqrt{3603}}{723002}i, \frac{30\sqrt{1084503}}{361501} \right) \right)$. Applying the LEB refinement process to this tetrahedron does not seem to lead to a finite orbit.*

The four tetrahedra given in Examples 3.3, 3.4, 3.5, and 3.6 have long and potentially unbounded orbits. The regular tetrahedron τ^R and cube corner tetrahedron τ^C have large orbits, but these orbits do not grow uncontrollably as shown in Table 2 since after $n = 40$ the orbits $\bigcup_{n=0}^{40} \Gamma_{\tau^R}^{(n)}$ and $\bigcup_{n=0}^{40} \Gamma_{\tau^C}^{(n)}$ contain 3793 and 2919 tetrahedra, respectively. In addition, the minimal face and dihedral angles seem to remain bounded by similar values.

In Theorem 3.4, we show that the orbit of the cube corner tetrahedron is actually included in that of the regular tetrahedron, explaining why the values obtained in the Table 2 are so close to each other and why minimal quantities for the cube corner are always larger than minimal quantities for the regular tetrahedron.

Theorem 3.4. *Assuming that the edge to be bisected is specified by our normalization procedure, the orbit of the cube corner tetrahedron is included in the orbit of the regular tetrahedron.*

Proof. It suffices to show how to reach the cube corner tetrahedron τ_C from the regular tetrahedron τ_R using the maps Φ_L and Φ_R . This can be done in 7 steps:

Table 2: We report the minimal dihedral angle, the minimal face angle and the minimal normalized volume of the tetrahedra in the orbits $\bigcup_{n=0}^{40} \Gamma_{\tau}^{(n)}$, where τ is one of the normalized tetrahedra from Examples 3.3, 3.4, 3.5 and 3.6. The initial values are given in parentheses.

Metric	Regular	Cube corner	Wedge	Needle
Minimal dihedral angle (deg)	15.52° (70.53°)	15.52° (54.74°)	8.05° (8.05°)	4.01° (60.08°)
Minimal face angle (deg)	11.63° (60°)	11.97° (45°)	5.71° (5.71°)	2.62° (5.72°)
Minimal normalized volume (%)	4.78% (100%)	4.78% (50%)	3.54% (5%)	0.30% (1.22%)
Number of shapes in the orbit after $n = 40$ iterations	3793	2919	12144	285592

1. Step 1: $\Phi_{L,R}(\tau^R) = \left(\frac{1}{4} + \frac{\sqrt{3}}{4}i, \left(\frac{1}{2} + \frac{\sqrt{3}}{6}i, \frac{\sqrt{6}}{3} \right) \right)$
2. Step 2: $\Phi_R \left(\left(\frac{1}{4} + \frac{\sqrt{3}}{4}i, \left(\frac{1}{2} + \frac{\sqrt{3}}{6}i, \frac{\sqrt{6}}{3} \right) \right) \right) = \left(\frac{1}{4} + \frac{\sqrt{3}}{4}i, \left(\frac{1}{2} + \frac{\sqrt{3}}{3}i, \frac{\sqrt{6}}{6} \right) \right)$
3. Step 3: $\Phi_L \left(\left(\frac{1}{4} + \frac{\sqrt{3}}{4}i, \left(\frac{1}{2} + \frac{\sqrt{3}}{3}i, \frac{\sqrt{6}}{6} \right) \right) \right) = \left(\frac{1}{2} + \frac{\sqrt{3}}{6}i, \left(\frac{1}{3} + 0i, \frac{\sqrt{2}}{3} \right) \right)$
4. Step 4: $\Phi_R \left(\left(\frac{1}{2} + \frac{\sqrt{3}}{6}i, \left(\frac{1}{3} + 0i, \frac{\sqrt{2}}{3} \right) \right) \right) = \left(\frac{1}{2} + \frac{\sqrt{2}}{4}i, \left(\frac{1}{2} + \frac{\sqrt{2}}{4}i, \frac{\sqrt{2}}{4} \right) \right)$
5. Step 5: $\Phi_{L,R} \left(\left(\frac{1}{2} + \frac{\sqrt{2}}{4}i, \left(\frac{1}{2} + \frac{\sqrt{2}}{4}i, \frac{\sqrt{2}}{4} \right) \right) \right) = \left(\frac{1}{4} + \frac{\sqrt{3}}{4}i, \left(\frac{1}{2} + \frac{\sqrt{3}}{6}i, \frac{\sqrt{6}}{6} \right) \right)$
6. Step 6: $\Phi_L \left(\left(\frac{1}{4} + \frac{\sqrt{3}}{4}i, \left(\frac{1}{2} + \frac{\sqrt{3}}{6}i, \frac{\sqrt{6}}{6} \right) \right) \right) = \left(\frac{1}{2} + \frac{1}{2}i, \left(\frac{1}{2} + 0i, \frac{1}{2} \right) \right)$
7. Step 7: $\Phi_{L,R} \left(\left(\frac{1}{2} + \frac{1}{2}i, \left(\frac{1}{2} + 0i, \frac{1}{2} \right) \right) \right) = \left(\frac{1}{2} + \frac{1}{2}i, \left(\frac{1}{2} + \frac{1}{2}i, \frac{\sqrt{2}}{2} \right) \right) = \tau^C.$

This concludes the proof, since we have shown how to reach τ^C from τ^R . \square

In Figure 10, we show how the metrics for the four tetrahedra studied here evolve under LEB. We do not report the results for the cube corner, since its orbit is included in that of the regular tetrahedron. For efficiency reasons, at each iteration we compute the different metrics on newly encountered shapes only. This is possible since we are computing the orbits symbolically. When the orbits are very large, the computational cost of computing everything symbolically is too high. In this case, we consider two tetrahedra to be the same numerically if every components of their normalized form are equal when rounded at 10 decimal places. This numerical procedure has been used to obtain the results for τ^W and τ^N . The number of shapes using this numerical approach has been validated by comparing it to the symbolic computations for the regular and cube corner tetrahedra and they lead to the same metrics and to the same number of shapes.

From Figure 10 we observe that the dynamics of the metrics for the regular tetrahedron seem to decrease and the minimum values reported in Table 2 occur towards the end of the simulation. While it is possible that these values continue to decrease, they seem to stabilize. The shapes produced by the wedge tetrahedron τ^N seem to become more regular and increasingly similar to that of the shapes produced by the regular tetrahedron τ^R . The fact that the minimal face and dihedral angles improve is best illustrated by noted that these minimal values are equal to their initial values, see Table 2.

The nearly degenerate needle tetrahedron τ^N is much less well-behaved. The number of shapes in $\bigcup_{n=0}^{40} \Gamma_{\tau^N}^{(n)}$ is much larger than that of the regular or cube corner tetrahedra, but still much smaller than the

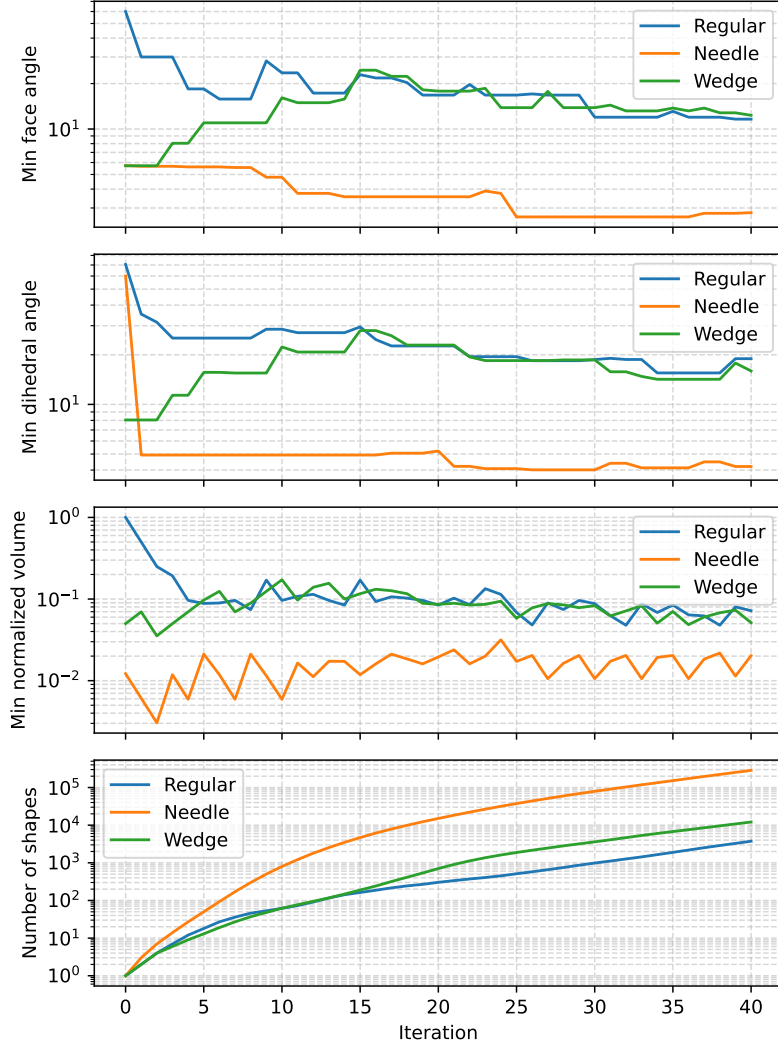


Figure 10: Dynamics of the metrics during the LEB process. The metrics at each iteration are computed on the set of new shapes produced at that iteration.

theoretical maximum number of shapes in such an orbit, which is $2^{41} - 1$. Even though the values for the minimal face angle and minimal dihedral angle are very small, they still seem to be bounded from below. Maybe a better sign that the shapes are not degenerating is the fact that the normalized volume of newly created shapes is increasing and the minimal value is obtained at iteration 2, see Figure 10. Note that while the minimal normalized volume in the orbit of τ^N is 0.30% of that of the regular tetrahedron, it is only a reduction by a factor of approximately 4 from the initial normalized volume of τ^N , which is 1.22%.

A visualization of the orbits of the regular tetrahedron and the needle tetrahedron is provided in Figures 11 and 12. A tetrahedron degenerates if either the red point corresponding to the base of the normalized tetrahedron becomes close to the x -axis or if the fourth vertex becomes close to the xy -plane. These gaps are clearly visible in Figure 11 but much less clear in the nearly degenerate needle tetrahedron case, see Figure 12.

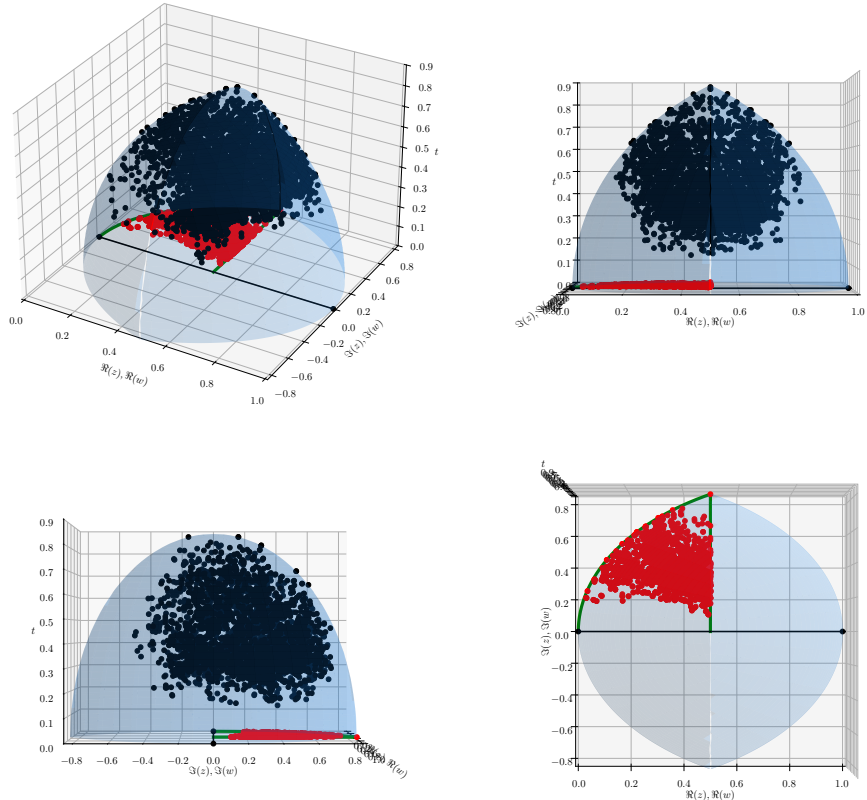


Figure 11: Visualization of the orbit of the regular tetrahedron after 40 iterations. The edges are not displayed to avoid having too much information in the figure and to better visualize the gap between the fourth vertex positions and the xy -plane. The bottom right panel shows only the positions of the base vertices.

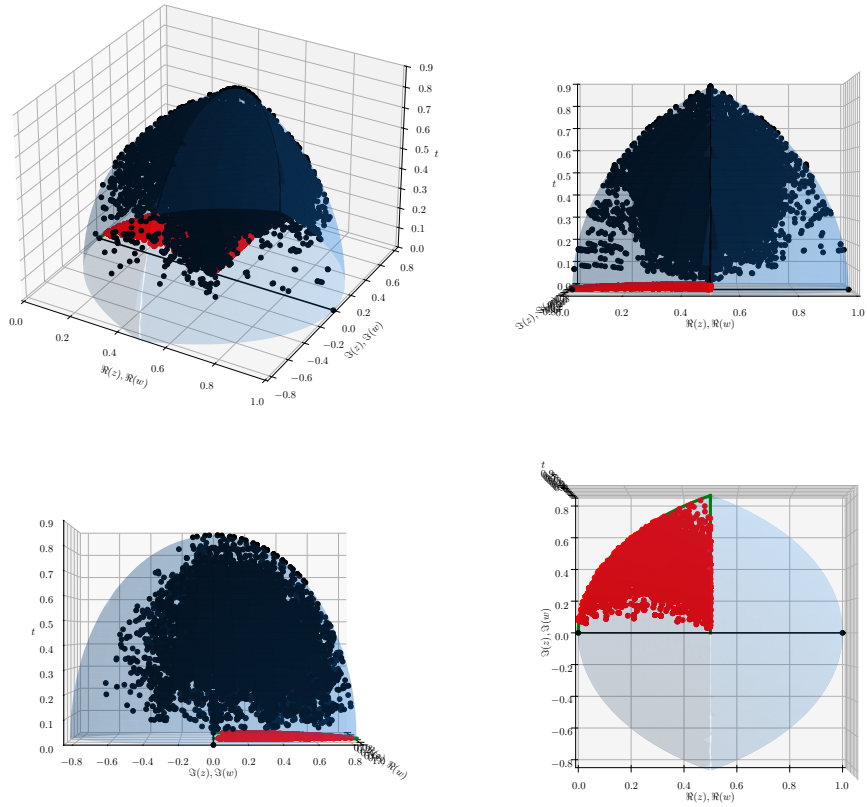


Figure 12: Visualization of the orbit of the needle tetrahedron after 20 iterations. The edges are not displayed to avoid having too much information in the figure and to better visualize the gap between the fourth vertex positions and the xy -plane. The bottom right panel shows only the positions of the base vertices.

4 Conclusions and future work

In this work, we have introduced a new normalization procedure for tetrahedra inspired by the works of Perdomo and Plaza [1,2]. This normalization procedure provides a geometric interpretation of the normalized form and allows for both an analytical and visual exploration of the orbits of tetrahedra under the LEB refinement algorithm. We show that the space-filling Sommerville tetrahedron essentially plays a central role in the dynamics of the LEB refinement method and that it has a very short orbit containing only 4 elements. Notably, three of these elements form a cycle. Small perturbations of the Sommerville tetrahedron lead to finite orbits clustering around this cycle. Looking at nearly regular tetrahedra as done in [14], we also find finite orbits clustering around a different limiting cycle not yet formally identified. Interestingly, we find many orbits longer than the theoretical bound of 37 introduced by Alder [21] and analyzed with a different normalization procedure in [20]. Overall, we have shown in Theorem 3.3 that there exist finite orbits of lengths $n \in \{3, 4, 7, 8, 13, 14\} \cup \{21, \dots, 26\} \cup \{36, 37, 38, 39, 42, 43, 44\}$ under the LEB.

However, there are also a number of tetrahedra whose orbits do not seem to be finite. We mention in this respect the cases of the regular tetrahedron, cube corner tetrahedron, wedge tetrahedron, and needle tetrahedron, studied in the present work. Nevertheless, there is a good indication that their orbits may be still attracted to a certain closed region, yet to be formally identified. Our results provide a complementary approach to that presented in [14–16, 20]. We use a different normalization procedure, but our results are highly compatible with theirs.

In the quest of proving the regularity of the tetrahedral partitions produced by the LEB refinements, we will develop our normalization procedure to provide a path for the development of the corresponding regularity proof in the spirit of the approach by Perdomo and Plaza [1,2]. For such a proof to work, we need to endow the space of tetrahedron \mathcal{T} with an appropriate metric. In Section 2, we introduced a possible choice of such a metric, see Definition 2.5. In the future work, we will explore the possibility to use that metric to identify closed regions in \mathcal{T} and to eventually construct the desired regularity proof for the LEB algorithm.

References

- [1] F. Perdomo, Á. Plaza, Proving the non-degeneracy of the longest-edge trisection by a space of triangular shapes with hyperbolic metric, *Applied Mathematics and Computation* 221 (2013) 424–432.
- [2] F. Perdomo, Á. Plaza, Properties of triangulations obtained by the longest-edge bisection, *Central European Journal of Mathematics* 12 (12) (2014) 1796–1810.
- [3] J. R. Shewchuk, What is a good linear element? interpolation, conditioning, and quality measures, in: 11th International Meshing Roundtable, {IMR} 2002, 2002, pp. 1–12.
- [4] M. Zlámal, On the finite element method, *Numerische Mathematik* 12 (1968) 394–409.
- [5] J. Brandts, S. Korotov, M. Křížek, On the equivalence of regularity criteria for triangular and tetrahedral finite element partitions, *Computers & Mathematics with Applications* 55 (10) (2008) 2227–2233.
- [6] J. Brandts, S. Korotov, M. Křížek, Generalization of the Zlámal condition for simplicial finite elements in \mathbb{R}^d , *Applications of Mathematics* 56 (5) (2011) 417–424.
- [7] M. Stynes, On faster convergence of the bisection method for all triangles, *Mathematics of Computation* 35 (152) (1980) 1195–1201.
- [8] M.-C. Rivara, Algorithms for refining triangular grids suitable for adaptive and multigrid techniques, *International Journal for Numerical Methods in Engineering* 20 (1984) 745–756.
- [9] M.-C. Rivara, New longest-edge algorithms for the refinement and/or improvement of unstructured triangulations, *International Journal for Numerical Methods in Engineering* 40 (1997) 3313–3324.
- [10] I. G. Rosenberg, F. Stenger, A lower bound on the angles of triangles constructed by bisection of the longest side, *Mathematics of Computation* 29 (130) (1975) 390–395.

- [11] M. Stynes, On faster convergence of the bisection method for certain triangles, *Mathematics of Computation* 33 (146) (1979) 717–721.
- [12] S. Korotov, M. Křížek, A. Kropáč, Strong regularity of a family of face-to-face partitions generated by the longest-edge bisection algorithm, *Computational Mathematics and Mathematical Physics* 48 (10) (2008) 1687–1698.
- [13] A. Hannukainen, S. Korotov, M. Křížek, On numerical regularity of the face-to-face longest-edge bisection algorithm for tetrahedral partitions, *Science of Computer Programming* 90 (2014) 34–41.
- [14] J. P. Suárez, A. Trujillo, T. Moreno, Computing the exact number of similarity classes in the longest edge bisection of tetrahedra, *Mathematics* 9 (12) (2021) 1447.
- [15] A. R. Trujillo-Pino, J. P. Suárez, M. A. Padrón, Finite number of similarity classes in longest-edge bisection of nearly equilateral tetrahedra, *Applied Mathematics and Computation* 472 (2024) 128631.
- [16] M. A. Padrón, Á. Plaza, J. P. Suárez, Similarity classes in the eight-tetrahedron longest-edge partition of a regular tetrahedron, *Mathematics* 11 (21) (2023) 4456.
- [17] D. Sommerville, Space-filling tetrahedra in Euclidean space, *Proc. Edinburgh Math. Soc.* 41 (1923) 49–57.
- [18] A. Meurer, C. P. Smith, M. Paprocki, O. Čertík, S. B. Kirpichev, M. Rocklin, A. Kumar, S. Ivanov, J. K. Moore, S. Singh, T. Rathnayake, S. Vig, B. E. Granger, R. P. Muller, F. Bonazzi, H. Gupta, S. Vats, F. Johansson, F. Pedregosa, M. J. Curry, A. R. Terrel, v. Roučka, A. Saboo, I. Fernando, S. Kulal, R. Cimrman, A. Scopatz, Sympy: symbolic computing in python, *PeerJ Computer Science* 3 (2017) e103.
- [19] R. Hošek, The role of Sommerville tetrahedra in numerical mathematics, *Programs and Algorithms of Numerical Mathematics* (2017) 46–54.
- [20] M. A. Padrón, A. Trujillo-Pino, J. P. Suárez, Convergence of the R_+^1 tetrahedra family in iterative longest edge bisection, *Mathematics and Computers in Simulation* 238 (2025) 555–567.
- [21] A. Adler, On the bisection method for triangles, *Mathematics of Computation* 40 (162) (1983) 571–574.
- [22] G. Aparicio, L. G. Casado, E. M. Hendrix, B. G.-Tóth, I. García, On the minimum number of simplex shapes in longest edge bisection refinement of a regular n -simplex, *Informatica* 26 (1) (2015) 17–32.

ID	Tetrahedron
τ_1	$\left(\frac{21}{76} + \frac{\sqrt{1079}}{76}i, \left(\frac{13}{19} + \frac{233\sqrt{1079}}{41002}i, \frac{\sqrt{260424203}}{41002}\right)\right)$
τ_2	$\left(\frac{53}{108} + \frac{\sqrt{1079}}{108}i, \left(\frac{61}{108} + \frac{7\sqrt{1079}}{116532}i, \frac{\sqrt{82239222}}{19422}\right)\right)$
τ_3	$\left(\frac{43}{88} + \frac{\sqrt{1759}}{88}i, \left(\frac{5}{11} + \frac{225\sqrt{1759}}{19349}i, \frac{\sqrt{491580694}}{38698}\right)\right)$
τ_4	$\left(\frac{20}{41} + \frac{3\sqrt{33}}{41}i, \left(\frac{39}{82} + \frac{20\sqrt{33}}{4059}i, \frac{\sqrt{17187159}}{8118}\right)\right)$
τ_5	$\left(\frac{55}{116} + \frac{\sqrt{2543}}{116}i, \left(\frac{27}{58} + \frac{1299\sqrt{2543}}{147494}i, \frac{\sqrt{936808141}}{73747}\right)\right)$
τ_6	$\left(\frac{39}{80} + \frac{\sqrt{1759}}{80}i, \left(\frac{1}{2} + \frac{41\sqrt{1759}}{3518}i, \frac{\sqrt{111722885}}{17590}\right)\right)$
τ_7	$\left(\frac{5}{17} + \frac{2\sqrt{15}}{17}i, \left(\frac{12}{17} + \frac{217\sqrt{15}}{4080}i, \frac{\sqrt{3239265}}{4080}\right)\right)$
τ_8	$\left(\frac{12}{25} + \frac{\sqrt{274}}{50}i, \left(\frac{59}{100} - \frac{2\sqrt{274}}{3425}i, \frac{\sqrt{1740311}}{2740}\right)\right)$
τ_9	$\left(\frac{1}{2} + \frac{\sqrt{15}}{12}i, \left(\frac{41}{96} + \frac{\sqrt{15}}{240}i, \frac{\sqrt{63515}}{480}\right)\right)$
τ_{10}	$\left(\frac{5}{17} + \frac{2\sqrt{15}}{17}i, \left(\frac{10}{17} + \frac{263\sqrt{15}}{4080}i, \frac{\sqrt{3239265}}{4080}\right)\right)$
τ_{11}	$\left(\frac{39}{80} + \frac{\sqrt{1759}}{80}i, \left(\frac{19}{40} + \frac{939\sqrt{1759}}{70360}i, \frac{\sqrt{111722885}}{17590}\right)\right)$
τ_{12}	$\left(\frac{47}{96} + \frac{\sqrt{1055}}{96}i, \left(\frac{13}{32} + \frac{29\sqrt{1055}}{33760}i, \frac{\sqrt{40204995}}{12660}\right)\right)$
τ_{13}	$\left(\frac{39}{80} + \frac{\sqrt{2319}}{80}i, \left(\frac{1}{2} + \frac{55\sqrt{2319}}{4638}i, \frac{\sqrt{147291285}}{23190}\right)\right)$
τ_{14}	$\left(\frac{55}{116} + \frac{\sqrt{2543}}{116}i, \left(\frac{14}{29} + \frac{622\sqrt{2543}}{73747}i, \frac{\sqrt{936808141}}{73747}\right)\right)$
τ_{15}	$\left(\frac{57}{116} + \frac{\sqrt{2319}}{116}i, \left(\frac{27}{58} + \frac{1187\sqrt{2319}}{134502}i, \frac{\sqrt{854289453}}{67251}\right)\right)$
τ_{16}	$\left(\frac{1}{2} + \frac{\sqrt{15}}{12}i, \left(\frac{55}{96} + \frac{\sqrt{15}}{240}i, \frac{\sqrt{63515}}{480}\right)\right)$
τ_{17}	$\left(\frac{5}{11} + \frac{\sqrt{274}}{22}i, \left(\frac{21}{44} + \frac{49\sqrt{274}}{6028}i, \frac{\sqrt{19143421}}{6028}\right)\right)$
τ_{18}	$\left(\frac{1}{2} + \frac{\sqrt{15}}{12}i, \left(\frac{41}{96} - \frac{\sqrt{15}}{240}i, \frac{\sqrt{63515}}{480}\right)\right)$
τ_{19}	$\left(\frac{23}{72} + \frac{\sqrt{1055}}{72}i, \left(\frac{7}{12} + \frac{97\sqrt{1055}}{12660}i, \frac{\sqrt{26803330}}{12660}\right)\right)$
τ_{20}	$\left(\frac{41}{86} + \frac{\sqrt{1243}}{86}i, \left(\frac{45}{86} - \frac{39\sqrt{1243}}{106898}i, \frac{\sqrt{678962647}}{53449}\right)\right)$
τ_{21}	$\left(\frac{5}{17} + \frac{2\sqrt{15}}{17}i, \left(\frac{41}{68} + \frac{287\sqrt{15}}{4080}i, \frac{\sqrt{3239265}}{4080}\right)\right)$
τ_{22}	$\left(\frac{6}{19} + \frac{\sqrt{274}}{38}i, \left(\frac{45}{76} + \frac{315\sqrt{274}}{20824}i, \frac{\sqrt{66131818}}{20824}\right)\right)$
τ_{23}	$\left(\frac{47}{96} + \frac{\sqrt{1055}}{96}i, \left(\frac{19}{32} - \frac{29\sqrt{1055}}{33760}i, \frac{\sqrt{40204995}}{12660}\right)\right)$
τ_{24}	$\left(\frac{5}{17} + \frac{\sqrt{274}}{34}i, \left(\frac{10}{17} + \frac{331\sqrt{274}}{18632}i, \frac{\sqrt{59170574}}{18632}\right)\right)$
τ_{25}	$\left(\frac{39}{80} + \frac{\sqrt{2319}}{80}i, \left(\frac{19}{40} + \frac{1219\sqrt{2319}}{92760}i, \frac{\sqrt{147291285}}{23190}\right)\right)$
τ_{26}	$\left(\frac{41}{86} + \frac{\sqrt{1243}}{86}i, \left(\frac{41}{86} + \frac{39\sqrt{1243}}{106898}i, \frac{\sqrt{678962647}}{53449}\right)\right)$
τ_{27}	$\left(\frac{12}{25} + \frac{\sqrt{274}}{50}i, \left(\frac{41}{100} + \frac{2\sqrt{274}}{3425}i, \frac{\sqrt{1740311}}{2740}\right)\right)$
τ_{28}	$\left(\frac{53}{108} + \frac{\sqrt{1079}}{108}i, \left(\frac{47}{108} - \frac{7\sqrt{1079}}{116532}i, \frac{\sqrt{82239222}}{19422}\right)\right)$
τ_{29}	$\left(\frac{5}{17} + \frac{2\sqrt{15}}{17}i, \left(\frac{47}{68} + \frac{193\sqrt{15}}{4080}i, \frac{\sqrt{3239265}}{4080}\right)\right)$
τ_{30}	$\left(\frac{41}{88} + \frac{\sqrt{2543}}{88}i, \left(\frac{21}{44} + \frac{1251\sqrt{2543}}{111892}i, \frac{\sqrt{710682038}}{55946}\right)\right)$
τ_{31}	$\left(\frac{57}{116} + \frac{\sqrt{2319}}{116}i, \left(\frac{15}{29} + \frac{566\sqrt{2319}}{67251}i, \frac{\sqrt{854289453}}{67251}\right)\right)$
τ_{32}	$\left(\frac{43}{88} + \frac{\sqrt{1759}}{88}i, \left(\frac{23}{44} + \frac{859\sqrt{1759}}{77396}i, \frac{\sqrt{491580694}}{38698}\right)\right)$
τ_{33}	$\left(\frac{20}{41} + \frac{3\sqrt{33}}{41}i, \left(\frac{43}{82} - \frac{20\sqrt{33}}{4059}i, \frac{\sqrt{17187159}}{8118}\right)\right)$
τ_{34}	$\left(\frac{19}{72} + \frac{\sqrt{1079}}{72}i, \left(\frac{49}{72} + \frac{473\sqrt{1079}}{77688}i, \frac{\sqrt{27413074}}{12948}\right)\right)$
τ_{35}	$\left(\frac{41}{88} + \frac{\sqrt{2543}}{88}i, \left(\frac{5}{11} + \frac{323\sqrt{2543}}{27973}i, \frac{\sqrt{710682038}}{55946}\right)\right)$
τ_{36}	$\left(\frac{1}{2} + \frac{\sqrt{15}}{12}i, \left(\frac{55}{96} - \frac{\sqrt{15}}{240}i, \frac{\sqrt{63515}}{480}\right)\right)$
τ_{37}	$\left(\frac{19}{72} + \frac{\sqrt{1079}}{72}i, \left(\frac{7}{12} + \frac{101\sqrt{1079}}{12948}i, \frac{\sqrt{27413074}}{12948}\right)\right)$
τ_{38}	$\left(\frac{21}{76} + \frac{\sqrt{1079}}{76}i, \left(\frac{45}{76} + \frac{613\sqrt{1079}}{82004}i, \frac{\sqrt{260424203}}{41002}\right)\right)$
τ_{39}	$\left(\frac{21}{68} + \frac{\sqrt{1055}}{68}i, \left(\frac{41}{68} + \frac{669\sqrt{1055}}{71740}i, \frac{\sqrt{227828305}}{35870}\right)\right)$

Table 3: List of tetrahedra in the orbit of T1 defined in Table 1.